Epigenetic suppression of interferon lambda receptor expression leads to enhanced HuNoV replication *in vitro*.

Sabastine E. Arthur*, Frédéric Sorgeloos*[#], Myra Hosmillo, and Ian G. Goodfellow[#].

Division of Virology, Department of Pathology, University of Cambridge, Addenbrooke's Hospital, Hills Road, Cambridge, CB2 0QQ, United Kingdom

[#]Corresponding authors.

* These authors contributed equally to this work.

Email: ig299@cam.ac.uk , frederic.sorgeloos@gmail.com

Keywords: Human norovirus replicon, microarray analysis, interferon lambda receptor (IFNLR1), DNA methylation, epigenetic reprogramming.

Running Title: Epigenetic reprogramming of norovirus harbouring cells

The authors declare no conflict of interests.

Abstract

Human norovirus (HuNoV) is the main cause of gastroenteritis worldwide yet no therapeutics are currently available. Here, we utilize a human norovirus replicon in human gastric tumor (HGT) cells to identify host factors involved in promoting or inhibiting HuNoV replication. We observed that an IFN-cured population of replicon-harboring HGT cells (HGT-cured) was enhanced in their ability to replicate transfected HuNoV RNA compared to parental HGT cells, suggesting that differential gene expression in HGT-cured cells created an environment favouring norovirus replication. Microarray analysis was used to identify genes differentially regulated in HGT-NV and HGT-cured compared to parental HGT cells. We found that the IFN lambda receptor alpha (IFNLR1) expression was highly reduced in HGT-NV and HGT-cured cells. All three cell lines responded to exogenous IFN-β by inducing interferon stimulated genes (ISGs), however, HGT-NV and HGT-cured failed to respond to exogenous IFN-λ. Inhibition of DNA methyltransferase activity with 5-aza-2'-deoxycytidine partially reactivated IFNLR1 expression in HGT-NV and IFN-cured cells suggesting that host adaptation occurred via epigenetic reprogramming. In line with this, ectopic expression of the IFN-λ receptor alpha rescued HGT-NV and HGT-cured cells response to IFN-λ. We conclude that type III IFN is important in inhibiting HuNoV replication in vitro and that the loss of IFNLR1 enhances replication of HuNoV. This study unravels for the first time epigenetic reprogramming of the interferon lambda receptor as a new mechanism of cellular adaptation during long-term RNA virus replication and shows that an endogenous level of interferon lambda signalling is able to control human norovirus replication.

Importance

Noroviruses are one of the most wide-spread causes of gastroenteritis yet we have no therapeutics for their control and we do not fully understand what cellular processes control viral replication. Recent work has highlighted the importance of type III interferon (IFN) responses in the restriction of viruses that infect the intestine. Here we analysed the adaptive changes required to support long term

replication of noroviruses in cell culture and found that the receptor for type III IFN is decreased in its expression. We confirmed that this decreased expression was driven by epigenetic modifications and that cells lacking the type III IFN receptor are more permissive for norovirus replication. This work provides new insights into key host-virus interactions required for the control noroviruses and opens potential novel avenues for their therapeutic control.

Introduction

With the introduction of the rotavirus vaccine, human norovirus (HuNoV) is now the main etiologic agent responsible for gastroenteritis worldwide (1–4). The disease, characterized by diarrhoea, nausea and vomiting is generally self-limiting in healthy adults. However, in immunocompromised, elderly patients and young children under the age of five, the disease can become chronic and sometimes lead to death mostly due to dehydration (5–9). Despite this and the profound economic burden of the disease (10), there are no therapeutics or licensed vaccines available.

Until the advent of the B lymphocyte-based and stem cell-derived human intestinal enteroid culture systems (11, 12), HuNoV research has been hampered by the lack of cell culture and small animal models recapitulating noroviral infection and pathogenesis. However, limitations in robustness, cost and labour intensity associated with both methods foreshadow that advances in HuNoV research still relies on the well-established murine norovirus (MNV) infection model and norovirus replicon systems (13, 14). These systems have been used to identify key host factors that impact the lifecycle of HuNoV, reviewed by Thorne and Goodfellow (15).

Contrary to the type I IFNs (IFN-α/β) which were discovered more than an half century ago (16), type III interferons (IFN-λ) were discovered only little over a decade (17, 18). Although both cytokine families possess similar functions, a few but crucial differences exist in their biology. Notably, both cytokines signal through distinct heterodimeric receptors with type I IFN signalling through the interferon alpha/beta receptor (IFNAR) composed of the IFNAR1 and IFNAR2 subunits and type III

IFN through the interferon lambda receptor (IFNLR) which consists of the interferon lambda receptor 1 (IFNLR1) and interleukin 10 receptor beta (IL10RB) subunits. Unlike the type I IFN receptor that is expressed on most cell types, expression of the IFNLR1 subunit is restricted to cells of the mucosal epithelium, neutrophils and human hepatocytes (19–21). Although the immune cells of the blood were also shown to express the IFNLR1 subunit, the receptor has been reported to lack the ability to respond to IFN-λ (22).

Expression of type I and III interferons is regulated at the transcriptional level and relies on the recognition of conserved pathogen-associated molecular patterns (PAMPs). Detection of these molecular signatures by extracellular and intracellular pattern recognition receptors triggers the coordinated activation of distinct signalling pathways responsible for the activation of IRF-3/7 and NF-κB transcription factors that are required for IFN gene transcription. Secreted IFN-λ then binds to the IFNLR and is thought to activate the Janus kinase 1 and tyrosine kinase 2. Subsequently, recruited signal transducer and activator of transcription 1 (STAT1) and STAT2 are activated through phosphorylation leading to the expression of IFN stimulated genes (ISGs), some of which have direct antiviral activities (23). Interferon lambdas are important players in both innate and adaptive immunity and have profound antiviral effects on a variety of viruses (24–28). Expression of IFNLR1 on epithelial cells of the small intestine and colon was shown to be important in IFN-λ-mediated antiviral activity against persistent MNV and reovirus infection *in vivo* (29). Treatment of persistently infected mice lacking adaptive immune response ($Rag1^{-/-}$) with IFN-λ abolished viral replication, suggesting that IFN-λ can cure persistent MNV infection in absence of adaptive immunity and this ability requires the expression of IFNLR1 (30). In line with this, the effect of antibiotics that inhibit persistent MNV infection in the gut has also been shown to be dependent on IFNLR1 expression as well as IRF3 and STAT1 transcription factors (31). It was observed that AG129 sentinel mice lacking the ability to respond to both IFN-α/β and IFN-γ housed together with MNV-infected mice developed a diarrhoea-associated MNV infection. Overexpression of IFN-λ in sentinel mice upregulated ISG expression, inhibited MNV replication in the small intestine and prevented them from being infected

99 when co-housed with MNV-infected mice (32). This article was submitted to an online preprint
100 archive (33).
101
102
103

Results

Generation and characterization of human cell lines bearing stable human norovirus replicons.

To understand the influence of viral and host factors involved in HuNoV replication, we sought to generate several human cell lines stably replicating HuNoV RNA. To this end, BHK-21 cells were transfected with capped Norwalk replicon RNA harbouring a neomycin selection marker (14) and subjected to G418 selection 48 hours after transfection (Fig. 1A). Although the vast majority of the cells died within one week, individual cell colonies were observed and subjected to limiting dilution. A single high-expressing clone was selected and expanded to generate stable replicon-containing BHK-21 cells (BHK-NV). VPg-linked RNA extracted from these cells was transfected into HGT cells, a cell line of epithelial origin which was subsequently selected on the basis of their G418 resistance in order to generate human norovirus replicon cells (HGT-NV). These HGT-NV cells were either collected as a population or subjected to limiting dilution to produce HGT-NV cell clones. The HGT-NV population was further passaged 16 times in the presence of IFN□α at a concentration of 1000 U/mL in the absence of G418 selection over an 8 weeks period leading to the generation of HGT-Cured cells. These cells were subsequently cultured in presence of G418 to observe their loss of resistance to G418 confirming the complete elimination of the replicon. Detection of HuNoV RNA by RT-qPCR analysis confirmed the presence of noroviral genomes in HGT-NV cells that were absent from HGT-Cured or parental HGT cells used as control (Fig. 1B). To confirm the presence of authentic steady-state replication of Norwalk RNA, cells were subjected to immunofluorescence analysis using monoclonal antibodies directed against dsRNA, a by-product assumed to be universally generated during viral replication (34, 35). As shown in Fig. 1C, punctate structures reminiscent of replication complexes were identified in HGT-NV cells while no signal above background levels was detected in HGT-Cured or in parental cell lines. Taken together these results suggest that HuNoV VPg-linked RNA successfully replicates in HGT cells and displays all the characteristics of a replication-competent RNA.

Cured population of HGT-NV cells demonstrate enhanced HuNoV replication.

Stable viral RNA replication under drug-mediated selection leads to an environment where on the one hand host cells face the selective pressure of the drug and, on the other hand, replicating RNA faces innate cellular responses aimed at inhibiting replication. This results in the establishment of a metastable equilibrium prone to adaptation from both cells and the replicating viral RNA. To test for the appearance of such adaptive mutation(s) in the replicon, VPg-linked RNA was extracted from BHK-NV and HGT-NV cells and subjected to consensus genome sequencing. Sequence analysis revealed that viral RNA originating from both BHK-NV and HGT-NV cells underwent many synonymous and non-synonymous genomic changes, suggesting the potential adaptation of HuNoV RNA to specific cellular environments (Supporting information Table 1). To test specifically for host cell adaptation, wild-type VPg-linked RNA extracted from BHK-NV cells was re-transfected in both HGT and HGT-Cured cell lines that were subsequently selected for 5 days with G418. As shown in Fig. 2A, HGT-Cured cells gave rise to a greater number of stable replicon colonies than parental HGT cells. To quantitatively confirm this observation, each cell line was transfected with wild-type VPg-linked RNA replicon and cells were harvested at various time points for RNA extraction and viral RNA quantification (Fig. 2B). From 5 days post transfection, the levels of Norwalk replicon RNA were significantly higher in HGT-Cured cells when compared to HGT cells. Noroviral RNA levels further increased at day 6 to yield a 15-fold difference between HGT-Cured and HGT cells. Quantification of transfected VPg-linked viral RNA at 6h post transfection revealed similar levels in both HGT and HGT-Cured cells suggesting that IFN treatment did not alter the ability of HGT-Cured cells to be transfected (data not shown). We thus concluded that HGT-Cured cells possess a greater degree of permissiveness to viral replication than parental HGT cells.

An alteration in cellular environment is responsible for enhanced viral replication in HGT-Cured cells.

Increased replication of HuNoV VPg-linked RNA in HGT-Cured cells suggests that these cells provide a better cellular environment compared to that of parental HGT cells. To get insights into the mechanism of this cell-derived HuNoV replicon permissiveness, genome-wide expression profiles from HGT, HGT-NV and HGT-Cured cell lines were quantified using Illumina BeadChip microarrays

(Tables S2 and S3). We first compared the gene expression profiles of HGT-NV cells relative to their HGT controls. As seen in Figure 3A, more than 2000 genes (HGT-NV-vs-HGT: 2074, HGT-Cured-vs-HGT: 858) were identified for which mRNA expression was significantly modified at a FDR lower than 0.01. Of these, a minority of 151 genes had expression changes in either direction greater than 2-fold suggesting that HuNoV replication has a marginal effect on the whole transcriptional landscape of replicon harbouring cells. Using the same criteria, comparison of gene expression profiles between HGT cells and HGT-Cured cells led to identification of 101 genes for which expression was differentially regulated between the two cell lines (Tables S4-S5). To confirm these observations and to probe for the accuracy of gene expression measured by microarray analysis, we first compared expression changes obtained by microarrays with that measured by RT-qPCR analysis. To this end, ten genes differentially regulated across conditions and spanning a wide range of fold changes were chosen for RT-qPCR validation (Fig. 3B). Globally, we observed a high correlation between the two techniques with Pearson's correlation coefficients ranging from 0.90 to 0.95. Direct comparison of raw microarray signal intensities with differences in cycle threshold obtained by real-time PCR displayed the same trends suggesting that similar fold changes were primarily the consequence of gene expression differences and were not an artefact resulting from different gene normalization techniques. Differential gene expression at the protein level of selected genes was further confirmed by western blot analysis (Fig. S1A-B). Taken together these data extensively confirms the reliability of gene expression measurements by microarray analysis.

The number of genes showing similar regulation between HGT-NV and HGT-Cured is surprisingly high and likely reflects cellular long-term adaption to replicating RNA (GO term enrichment analysis did not reveal specific pathway enrichment in this gene set). Remarkably, we observed an opposite regulation of several interferon-stimulated genes (ISGs) when comparing the HGT-NV transcriptional landscape with that of parental HGT cells (Fig. 3C and Table S4). While genes coding for IFITM2, IFITM3, IFIH1 and IFI27L2 were down-regulated, IFIT1 and IFIT2 genes were significantly up-regulated in HGT-NV cells. Expression of IFIT1 and IFIT2 proteins is known to be IRF3-dependent (36, 37), while expression of IFITMs and IFIH1 genes was shown to be mediated by ISRE binding

(38, 39), this suggests that while HuNoV replication induces IRF3-dependent immune responses, activation of ISRE-dependent genes located downstream in the interferon signalling pathway is inhibited. In line with this observation, microarray analysis identified a statistically significant down-regulation of the type III interferon receptor (IFNLR1) expression in HGT-NV and HGT-Cured cells when both were compared to HGT cells. To confirm and extend this observation, we compared IFNLR1 and IL10RB gene expression by quantitative RT-PCR. Remarkably, we found more than 20-fold decrease in IFNLR1 expression when parental HGT cells were compared to HGT-NV or HGT-Cured cells. In contrast, no significant difference was observed when IL10RB gene expression was measured (Fig. 3D-E).

Sensing of cytosolic RNA and DNA PAMPs by the innate immune system is functional.

To examine whether HGT-NV and HGT-Cured cells were able to detect and mount an innate immune response against cytosolic PAMPs, poly (I:C) and poly (dA:dT) were transfected in the various HGT-derived cell lines and viperin expression levels were measured by RT-qPCR (Fig. 4A-B). Although the cell lines exhibited upregulation of viperin mRNA to various extents, a significant increase of viperin expression above basal levels was detected in all the three cell lines in response to both poly(I:C) and poly(dA:dT). Given that the overall levels of viperin following treatment was comparable across the three cell lines, evident by the relative ratio with respect to β-actin, we concluded that PAMP sensing and downstream signalling pathways are functional in these cell lines.

The ability to respond to type III but not type I IFN in HGT-NV and HGT-Cured cells is debilitated.

We next investigated the ability of type I and type III interferons to elicit ISGs induction. To this end, cells were incubated with human IFN-β or IFN-λ2 for 16 hours and viperin expression levels were measured by RT-qPCR. We observed that viperin mRNA was readily induced in all three cell lines in response to exogenous type I IFN (IFN-β) treatment (Fig. 5A). However, whereas HGT cells responded to exogenous type III IFN (IFN-λ2) treatment, HGT-NV and HGT-Cured cells did not (Fig. 5B). To test whether the absence of ISG expression is linked to a defect of STAT1

phosphorylation in response to type I or type III interferons, cells were incubated with either recombinant IFN-β or IFN-λ2 and STAT1 phosphorylation status was analysed by western blot using anti-STAT1 phospho-specific antibodies. We observed that although STAT1 was phosphorylated in all cell lines following IFN-β treatment (Fig. 5C), no STAT1 phosphorylation was detected in HGT-NV and HGT-Cured cells following IFN-λ2 treatment (Fig. 5D). To ensure that the absence of STAT1 phosphorylation in HGT-NV cells is not due to a potential clonal effect, different clones as well as a population of the HGT-NV cells were included in the experiment. Similarly, the clones represented here by clone 2 (C2) and the polyclonal cell population responded to IFN-β but not to IFN-λ2 (Fig. 5E-F). Taken together, these results indicate that signal transduction induced by type I IFN is intact while STAT1 phosphorylation induced in response to lambda interferon is inhibited in HGT cells that sustained HuNoV replication.

IFNLR1 overexpression rescues STAT1 phosphorylation in response to IFN lambda.

To directly test whether the down-regulation of IFNLR1 expression measured in HGT-NV and Cured cells is responsible for their unresponsiveness to lambda interferon, cells were transfected with an IFNLR1-expressing plasmid and stimulated with IFN-λ2 the day after. We observed that IFNLR1 expression rescued STAT1 phosphorylation in response to interferon lambda suggesting that IFNLR1 down-regulation in HGT-NV and HGT-Cured cells is responsible for IFN-λ insensitivity (Fig. 6). In addition, this experiment shows that the JAK-STAT signalling cascade comprising JAK1, Tyk2 and possibly JAK2 (40) is functional and leads to the phosphorylation of STAT1.

Inactivation of interferon type I and III receptors increases HuNoV replication in epithelial cells.

To directly test the influence of type I and type III IFNs on HuNoV replication, HGT cells lines deficient either for the interferon alpha/beta receptor IFNAR1 or for the interferon lambda receptor IFNLR1 were generated using CRISPR/Cas9-mediated genome editing. To this end, parental HGT cells were transduced with lentiviruses expressing IFNAR1 or IFNLR1 single guide RNAs and clonally selected in the presence of puromycin. Individual clones were screened for gene inactivation

by IFN-β or IFN-λ2 challenging followed by analysis of STAT1 phosphorylation by western-blot and viperin induction by RT-qPCR (Fig. S2A-B). VPg-linked viral RNA was then transfected and cells were selected in the presence of 0.5mg/mL G418 for up to 6 days. Relative to day 0 taken as reference, we observed a significant increase in genomic viral RNA in all cell lines with the exception of parental HGT cells corroborating the antiviral activity of both type I and type III IFNs on HuNoV replication (Fig. 7). Similarly, an increased ability of modified cell lines to promote colony formation induced by the HuNoV replicon was observed (data not shown).

IFNLR1 promoter is methylated in HGT-NV and HGT-Cured cells.

The dimeric interferon lambda receptor consists of the ubiquitously expressed IL10RB chain subunit and the interferon lambda specific chain IFNLR1 whose expression is limited to cells of epithelial origin (20). Cell-type specific expression of the IFNLR1 subunit was later shown to be inversely correlated with the methylation of its promoter (41). To examine whether viral replication induced, or lead to the selection of, alterations of IFNLR1 gene expression through epigenetic modifications, cells were incubated in the presence 5-aza-2'-deoxycytidine (5azadC), a deoxynucleoside analogue that strongly inhibits DNA methyltransferase (DNMT) activity. As shown in Fig. 8A, we observed a significant 6-fold increase of IFNLR1 mRNA levels in HGT-NV cells when compared to cells incubated with the vehicle only. A statistically significant increase in IFNLR1 gene expression was also observed in the case of HGT-Cured cells but to a lower extent (2.8-fold). In contrast, no change in IL10RB expression was detected when the same cells were incubated with 5azadC (Fig. 8B). In addition, incubation in the presence of MS-275 alone (an HDAC inhibitor) or in combination with 5azadC did not result in increased IFNLR1 expression when compared to 5azadC alone suggesting that the presence of replicating HuNoV did not modify the chromatin structure of the IFNLR1 gene (data not shown). Taken together, these results suggest that the replication of HuNoV in HGT epithelial cells induces a long-term transcriptional silencing of the IFNLR1 gene through the methylation of its promoter.

Discussion

The purpose of this study was to compare genome-wide transcriptional responses of epithelial cells supporting autonomous HuNoV replication with those elicited by IFN-cured derivatives showing increased viral replication abilities. We found that the interferon lambda receptor is downregulated in cells that sustained HuNoV replication. Mechanistically, this down-regulation of IFNLR1 was mediated by gene methylation as treatment with 5azadC, a DNA methyltransferase inhibitor, rescued the phenotype. This suggests that the lambda IFN pathway is a key constituent of the innate intrinsic defence against human norovirus and shows that an endogenous IFN lambda signalling activity is able to modulate the replication of the virus.

Influence of lambda interferons on murine noroviruses has been highlighted in previous studies using different experimental setups (29, 42, 43). In the case of the human norovirus, recent work using the same replicon in Huh-7 human hepatoma cell line showed that all three types of IFN, when exogenously added, were able to inhibit HuNoV replication leading to virus clearance during long-term treatment (44). However, it is not known whether physiological activation of the interferon pathways, particularly, the lambda IFN signalling pathway exerts an antiviral effect against human noroviruses. The present results add further evidence for the involvement of type III IFN in the control of human noroviruses, but extend earlier findings, by showing that physiological levels of type III IFN signalling can effectively restrict HuNoV replication. One of the major concerns with replicon systems is that gene expression landscapes might reflect clonal selection of RNA-replicating cells rather than a universal impact of viral replication on cellular gene expression. To exclude that differences in gene expression were exclusive to a specific cell type or population, we compared our dataset with previous genome wide-transcription profiles from Huh-7 hepatoma cells supporting autonomous replication of HuNoV RNAs (45). We found a (significant) positive correlation between the two datasets when statistically differentially expressed genes were compared ($r=0.19$; $p=0.03$; $n=113$) (or $r=0.49$; $p=0.1$; $n=12$, $FC>2$), suggesting that analogous cellular responses were induced in response to HuNoV replication in both cell lines.

It is interesting to note that IFNLR1 is also down-regulated in HGT-NV cells which have not been treated with exogenous type I IFN. This indicates that in the absence of selective pressure mediated by

type I IFN, modulation of the type III IFN pathway is preferentially selected over other genes with antiviral properties as exemplified in other studies using RNA replicons with selectable marker. For example, in the case of HCV replicon systems, several antiviral genes including *Viperin* and *MX1* were shown to be silenced through gene methylation, rendering Huh-7 cells permissive to HCV replication (46, 47).

An important observation in this study is the upregulation of several IRF3-dependent genes when HGT-NV cells were compared to parental HGT cells. As IRF3 activation is essential for type I and III interferon induction, upregulation of IRF3-dependent genes suggests that HuNoV replication produces PAMPs that are sensed by RIG-I like receptor(s) which in turn activate the cell-intrinsic immune signalling pathways. Similarly, down-regulation of ISRE-dependent genes in HGT-NV when compared to HGT-Cured cells, which have silenced the IFNLR1 gene to the same extent, put forward the idea that HuNoV replication induces IFN-dependent responses. In line with this, a recent study using the same replicon identified RIG-I and MDA5 proteins as potent negative regulator of HuNoV replication suggesting that viral RNA secondary structures can readily be detected during replication (Dang et al., 2018). These observations are however in striking contrast to the study of Qu and colleagues in which transfection of stool-derived HuNoV RNA readily replicated in 293T cells but failed to induce detectable interferon responses (48). Differences in experimental setups such as including cell lines, virus strains, stable versus transient viral replication and IFN response readouts may account for this discordant observation. Investigating whether diverse strains of HuNoV induce interferon responses in cell-derived human intestinal enteroids will be of interest to probe the influence of HuNoV replication on IFN induction and responses.

Increased replication of HuNoV in HGT-cured compared to either IFNAR and IFNLR1 knock-out cells suggests that differentially regulated genes other than IFN receptors may favour virus replication. However, manual curation of genes differentially regulated between parental and IFN-cured cells did not reveal individual genes convincingly known to modulate viral replication other than IFNLR1 and genes involved in the biosynthesis and trafficking of cholesterol. This suggests

317 either that a low but collective influence of these genes contributes to the increased replication of
318 HuNoV observed in HGT-Cured cells, or that some of the differentially expressed genes identified
319 have a potent yet unknown proviral activity towards the human norovirus.

320

321 Overall, our results provide insights into the interactions between the human norovirus and innate
322 cellular responses and show that endogenous levels of λ-IFNs control HuNoV replication suggesting
323 that they may have a therapeutic potential in the treatment of noroviral infections. In addition, the
324 high confidence gene expression datasets provided with this study is expected be useful for the
325 selection and examination of new targets aimed to antiviral therapy.

326
327 **Methods**

328

329 **Cells and Media**

330 Human gastric tumour (HGT) cells, human norovirus replicon-harbouring HGT (HGT-NV) cells and
331 IFN-α interferon-treated HGT-NV cells (HGT-Cured) were maintained in Dulbecco's minimal
332 essential medium supplemented with 10% fetal calf serum, 2 mM glutamine, 100 U/ml penicillin, 100
333 µg/ml streptomycin, 1X non-essential amino acid and 0.5 mg/ml G418 in the case of HGT-NV cells.
334 The DNA methyltransferase inhibitor 5-Aza-2′-deoxycytidine (Sigma-Aldrich, A3656) was diluted in
335 sterile water and used at a final concentration of 10 µM.

336 **Microarray analysis**

337 Four lineages of HGT, HGT-NV and HGT-Cured cells were grown in tissue culture flasks in the
338 appropriate culture media. After four successive passages, total RNA was extracted using TRIzol®
339 (Invitrogen). Microarray analysis was done using the HumanHT-12 v4 Expression BeadChip
340 (Illumina, Chesterford, UK). All microarray experiments, data normalizations and preliminary
341 analysis were fulfilled by the Cambridge Genomic Services, UK.

342 **Quantitative RT-PCR analysis**

343 Total cell RNA was extracted using a GenElute Mammalian Total RNA Miniprep kit (Sigma) and
344 contaminating genomic DNA was removed through RNase-free DNase I treatment (Roche). Total
345 RNA was then reverse transcribed using random hexamers and the M-MLV RT enzyme (Promega).
346 SYBR green-based quantitative PCR was performed using gene-specific primers listed in
347 (Supporting information Table 6). Each experimental condition was measured in biological triplicate
348 and results are shown as a ratio to levels detected in control cells according to the ΔΔCt method (49).
349 Additional non-template and non-reverse transcriptase samples were analysed as negative controls.
350 Data were collected using a ViiA 7 Real-Time PCR System (Applied Biosystems). Genomic viral
351 RNA was quantified by one step RT-qPCR using GI NV-specific primers. Viral genome copy
352 numbers were calculated by interpolation from a standard curve generated using serial dilutions of
353 viral RNA transcribed from the pNV101 plasmid coding for the full-length Norwalk genome (50).

354

355 **Nucleic acid transfection and IFN treatment**

356 Transfections of plasmid DNA or purified viral RNA (NV replicon) were carried out using
357 Lipofectamine 2000 (Invitrogen) according to manufacturer's instructions. Briefly, cells were seeded
358 in antibiotic-free growth medium at a density of 2×10^5 or 1×10^6 cells per well in 24- or 6-well plates,
359 respectively, and incubated overnight at 37°C. Lipofectamine 2000 reagent was diluted in Opti-
360 MEM® (Gibco) and incubated for 5 minutes at 25°C. After the incubation, plasmid DNA or viral
361 RNA, diluted in Opti-MEM® (Gibco), was mixed with the Lipofectamine: Opti-MEM mixture,
362 vortexed briefly and incubated at 25°C for 20 minutes. The DNA or RNA complex was subsequently
363 inoculated onto 80-90 % confluent cell monolayers, followed by incubation at 37°C. For viral RNA
364 transfection, media was replaced after 24 h with fresh complete growth medium containing G418 at a
365 concentration of 0.5 mg/ml. For IFN treatments, cells were seeded as described above and incubated
366 at 37°C for indicated time-points with or without recombinant type I IFN (IFN-β; Peprotech, Cat

N°:300-02BC), or type III IFN (IFN-λ2; Peprotech, Cat N°:300-02K) at a final concentration of 0.1 ug/ml.

Immunofluorescence microscopy

Cells were plated on 12 mm glass coverslips and allowed to adhere overnight before fixation with 4% paraformaldehyde in PBS. Cells were then permeabilized for 5 min with PBS-Triton X-100 0.2% and unspecific antigens were blocked for 1h using 2% normal goat serum (Sigma-S2007) in PBS-Tween-20 0.1% (PBST). Cells were then incubated for 1h with primary mouse monoclonal J2 anti-dsRNA antibodies in PBST at a dilution of 1:1000 (J2, SCICONS English & Scientific Consulting, Hungary). After extensive washes with PBST, species-matched AlexaFluor-conjugated secondary antibodies (ThermoFisher Scientific, A-11029) were added at a dilution of 1:500 in PBST for one additional hour. Coverslips were extensively washed and mounted on slides with Mowiol supplemented with DAPI and DABCO. Confocal micrographs were acquired on a Leica TCS SP5 confocal fitted with a 63x 1.3NA oil immersion objective using 405nm and 488nm laser excitation lines under sequential channel scanning to prevent fluorophore bleed-through artefacts due to spectral overlap.

Western blot analysis

Cell lysates were prepared in radio-immuno precipitation assay buffer (RIPA: 150 mM NaCl, 0.5% sodium deoxycholate, 0.1% SDS, 1mM EDTA, 1% Triton X-100, and 50 mM Tris pH8) supplemented with protease and phosphatase inhibitors (Calbiochem; Cat N°: 539134 and 524625). Protein concentrations were determined by BCA assay (Thermo Fisher Scientific). Equal amounts of total proteins were resolved by SDS-PAGE and transferred to nitrocellulose membranes. Blocking of unspecific antigens was carried out in 5% non-fat dried milk or 5% BSA in PBST for 1 h at 4°C. Primary antibodies were diluted in blocking buffer and incubated overnight at 4°C with gentle rocking (Supporting information Table 7). Membranes were washed three times in PBST for 5 min at RT. Species-matched IRDye-800CW secondary antibodies were diluted in blocking buffer as before and incubated at RT for 1 h. Membranes were washed again three times in PBST for 5 min at RT. Fluorescent signal was detected through an Odyssey CLx infrared imaging system (Li-COR).

393 **Generation of IFNAR1 or IFNLR1 knockout HGT cells**

394 HGT cells knockout for IFNAR1 or IFNLR1 genes were generated using the CRISPR/Cas9 system.
395 Lentivirus vectors encoding single-guide RNAs against IFNAR1 or IFNLR1 were generously
396 provided by Dr Steeve Boulant and are described in Pervolaraki et al. (51). Vesicular stomatitis virus
397 G-protein-pseudotyped lentiviral particles were generated by transient transfection of 293T cells
398 grown in 6-well plates using 1.25 µg lentiviral vector, 0.63 µg pMDLg/pRRE (Addgene #12251),
399 0.31 µg pRSV-Rev (Addgene #12253) and 0.38 µg pMD2.G (Addgene #12259) per well. Parental
400 HGT cells were transduced with lentiviral supernatants and incubated for 48 h. Transduced cells were
401 then selected on the basis of their resistance to puromycin at a concentration of 2.5 µg/mL. Clonal
402 isolation was performed by limiting dilution into 96-well plate at a density of 0.3 cell per well and
403 single cell clones were selected on the basis of visual examination. Single cell clones were expanded
404 and tested for IFNAR1 or IFNLR1 gene disruption by RT-qPCR measurement of viperin induction
405 following incubation with IFN-β or IFN-λ2, respectively. Absence of STAT1 phosphorylation
406 following incubation with receptor-matched interferons confirmed the gene ablation.

407 **Statistical analysis and data sharing**

408 Statistical significance was determined from experiments where $n \geq 3$ using two-tailed Student *t* tests
409 in Prism 6.0 (GraphPad). All microarray expression data reported in this study have been deposited
410 into Gene Expression Omnibus (GEO, http://www.ncbi.nlm.nih.gov/geo) with the accession number
411 GSE111041.

412

413 **Figure legends**

414 **Figure 1.** Generation and characterization of stable HuNoV replicons in HGT and U2OS cell lines.

415 A. Diagram showing the steps used to generate the various cell lines carrying human norovirus
416 replicons and their IFN-cured counterparts.

417 B. Total cellular RNA was extracted from each cell line and viral RNA quantified by RT-qPCR. Viral
418 RNA copy numbers were normalized to the total input RNA and expressed as genome equivalents/µg
419 of input RNA. The error bars represent the standard deviation determined from four biological
420 replicates. Viral RNA copy numbers were below the limit of detection in both HGT and HGT-Cured
421 cells. The dotted line represents the low limit of detection.

422 C. Detection of viral replication complexes by confocal imaging. Representative merged confocal
423 micrographs showing the detection of dsRNA (green) in indicated cell lines. Nuclei were stained with
424 DAPI (blue). Scale bars correspond to 20µm.

425 **Figure 2.** HGT-Cured cells demonstrate enhanced HuNoV replication.

426 A. HGT and HGT-Cured cells were transfected with VPg-linked replicon RNA. After five days of
427 selection with G418 at a concentration of 0.5 mg/mL, cellular morphology was analysed by light
428 microscopy.

429 B. Cells transfected with VPg-linked RNA were harvested at various time points post-transfection for
430 total RNA extraction and viral RNA was quantified by RT-qPCR. Viral RNA levels were determined
431 by comparison to a standard curve and normalized to the RNA input. The data are presented as mean
432 and standard deviation from three replicates. Indicated values are expressed as fold change in genome
433 equivalent normalized to viral RNA levels at 6 hours post-transfection to control for transfection
434 efficiency. Unpaired two-tailed Student's t-test was used to evaluate the statistical significance.

435

436 **Figure 3.** Microarray analysis and validation of differentially regulated genes between HGT-NV,
437 HGT-Cured and parental HGT cells.

438 A. Volcano plots of differentially expressed genes from microarray analysis comparing gene
439 expression in HGT-NV or HGT-Cured compared to parental HGT cells. Significantly up- or down-
440 regulated genes (FDR<0.01 and $|\log_2$ fold change$| \geq 1$) are represented in red or green, respectively.

441 B. Fold change correlation between microarray analysis and quantitative real-time PCR (RT-qPCR).
442 Scatter plots comparing $\log_2$ fold changes of selected genes measured by microarray analysis and RT-
443 qPCR in HGT-NV or HGT-Cured compared to parental HGT cells. Error bars represent the standard
444 deviation of biological quadruplicate experiments analyzed in triplicate reactions. The Pearson
445 correlation coefficient (r) and the number of pairs analysed (n) are indicated on each graph. Dotted
446 lines illustrate the 95% confidence interval of the linear regression.

447 C. Venn diagrams representing the overlap of significantly up- and down-regulated genes between
448 HGT-NV or HGT-Cured cells compared to parental HGT cells. The top ten genes within each
449 category are shown.

450 D-E. IFNLR1 (D) but not IL10RB (E) gene expression is down-regulated in HGT-NV and HGT-
451 Cured cells. Changes in gene expression of IFNLR1 and IL10RB mRNA levels were normalized to β-
452 actin levels and calculated using the $\Delta\Delta C_T$ method. Relative expression was determined from one
453 experiment performed in biological triplicate and compared to the expression levels measured in HGT
454 control. Statistical significance was determined using the unpaired *t* test. Error bars represent the
455 standard deviation between biological replicates.

456

457 **Figure 4.** Innate immune responses to RNA and DNA PAMPs are functional.

458 Cells were transfected with poly (I:C) (A) or poly (dA:dT) (B) and total RNA was harvested 8h post-
459 transfection for quantification of viperin mRNA levels by RT-qPCR. Viperin mRNA levels were
460 expressed as differences of cycle threshold (C_t) of viperin, relative to the C_t of beta-actin. The error
461 bars represent standard deviation, determined from the result of three replicates.

462

463 **Figure 5.** The ability to respond to type III but not type I IFN is debilitated in HGT-NV and HGT-
464 Cured cells.

Cells were treated with type I (IFN-β) (A) or type III interferon (IFN-λ2) (B), incubated overnight and harvested for total RNA extraction and quantification of viperin mRNA levels by RT-qPCR. Viperin mRNA expression levels were expressed as differences of cycle threshold (C_t) of viperin, relative to the C_t of beta-actin. The error bars represent the standard deviation, determined from the result of three replicates.

(C-F) Western-blot analysis showing STAT1 phosphorylation after stimulation with type I and type III interferons in HGT, HGT-NV and HGT-Cured cell lines (C, E). HGT-NV Clone 2 (C2) and population of cells (pop) were included in the experiment (D, F). GAPDH was used as loading control.

Figure 6. Overexpression of IFNLR1 in HGT-NV and HGT-Cured cells rescues the ability to respond to type III IFN and the loss of the receptor enhances viral RNA replication in HGT cells.

HGT, HGT-NV and HGT-Cured were transfected with IFNLR1 expressing plasmid and STAT1 phosphorylation was measured in whole cell lysate by western blot after incubating cells with type III IFN for 15 min (A). STAT1 was used as a positive control and GAPDH was used as the loading control. HGT IFNLR1$^{-/-}$ cells transfected with GI viral VPg-linked RNA were harvested at 0 and 5 days post-transfection for total RNA extraction and viral RNA was quantified by RT-qPCR (B). The viral RNA levels were determined by comparing to a standard curve and normalized to the total input RNA. The data are presented as the mean and standard deviation from at least 11 replicates and are expressed as fold change in genome equivalent at day 0.

Figure 7. Genetic ablation of IFNAR1 and IFNLR1 interferon receptors promotes HuNoV replication.

Parental HGT, IFNAR1 and IFNLR1 knock-out cells were transfected with VPg-linked replicon RNA and submitted to G418 selection. Total cellular RNA was harvested at various time points post-

transfection and viral RNA was quantified by RT-qPCR. Relative viral replication was determined from one experiment performed in biological triplicate and compared to the replication levels measured in HGT control at day 0. Statistical significance was determined using the unpaired *t* test. Error bars represent the standard deviation between biological replicates.

Figure 8. IFNLR1 promoter is methylated during long-term HuNoV replication.

HGT, HGT-NV and HGT-Cured cells were incubated in the presence of 10 uM 5azadC for 72 hours or left untreated. Total cell RNA was extracted and IFNLR1 and IL10RB expression was measured by RT-qPCR. Total cellular RNA was harvested 72 hours post-treatment and IFNLR1 and IL10RB mRNA were quantified by RT-qPCR. Relative gene expression was determined from one experiment performed in biological triplicate and compared to the expression levels measured in corresponding untreated cells. Statistical significance was determined using the unpaired t test. Error bars represent the standard deviation between biological replicates.

Supplementary figure legends

Figure S1. Expression change validation of selected genes at the transcription and translation levels.

A. Direct comparison between microarray signal intensities and difference in cycle thresholds for *ANXA1* and *IFITM*3 genes.

B. Validation by western-blot analysis of ANXA1 and IFITM3 protein levels in HGT, HGT-NV and HGT-Cured cell lines. The indicated ratios represent the ANXA1 or IFITM3 protein levels normalized to the corresponding GAPDH loading controls relative to parental HGT cells.

Figure S2. Western blot validation of CRISPR/Cas9-induced knockout cells.

A-B. HGT wild-type cells as well as IFNAR1 (A) and IFNLR1 (B) CRISPR/Cas9 clones were treated with type I (IFN-β) (A) or type III interferon (IFN-λ2) (B) for 15 min and STAT1 phosphorylation (pT701) was measured by immunoblot analysis. GAPDH was used as a loading control.

Funding information

I.G. is a Wellcome Senior Fellow and this work was supported by funding from the Wellcome Trust (Ref: 207498/Z/17/Z). F.S. was funded by a Biotechnology and Biological Sciences Research Council (BBSRC) sLoLa grant (BB/K002465/1). S.A.E. is supported through a Cambridge Trust Cambridge-Africa PhD studentship. The funders had no role in study design, data collection and interpretation, or the decision to submit the work for publication

Author contributions

S.A.E., F.S., M.H., and I.G. designed, performed the research and analysed the data. S.A.E., F.S., and I.G. wrote the manuscript.

Acknowledgements

We thank Laure Dumoutier (de Duve Institute, Universite Catholique de Louvain) for the gift of the IFNLR1 (LICR2) expressing plasmid. We thank K Green (NIH, Bethesda) and KO Chang for the provision of pNV-Neo.

Conflicts of interest

The authors declare that they have no conflict of interest.

References

1. **Fankhauser RL**, **Noel JS**, **Monroe SS**, **Ando T**, **Glass RI**. 1998. Molecular Epidemiology of "Norwalk□like Viruses" in Outbreaks of Gastroenteritis in the United States. J Infect Dis **178**:1571–1578.

2. **Mawatari M**, **Kato Y**. 2014. Norovirus Gastroenteritis. Emerg Infect Dis Clin Case Stud **361**:203–212.

3. **Hall AJ**, **Lopman BA**, **Payne DC**, **Patel MM**, **Gastañaduy PA**, **Vinjé J**, **Parashar UD**. 2013. Norovirus disease in the united states. Emerg Infect Dis **19**:1198–1205.

4. **Lopman B**, **Ahmed SM**, **Robinson A**, **Verhoef L**, **Koopmans M**, **Hall AJ**. 2013. The global prevalence of norovirus among cases of gastroenteritis. Bangkok, Thail Vaccines Enteritis Dis.

5. **Ludwig A**, **Adams O**, **Laws HJ**, **Schroten H**, **Tenenbaum T**. 2008. Quantitative detection of norovirus excretion in pediatric patients with cancer and prolonged gastroenteritis and shedding of norovirus. J Med Virol **80**:1461–1467.

6. **Patel MM**, **Widdowson MA**, **Glass RI**, **Akazawa K**, **Vinjé J**, **Parashar UD**. 2008. Systematic literature review of role of noroviruses in sporadic gastroenteritis. Emerg Infect Dis **14**:1224–1231.

7. **Phillips G**, **Tam CC**, **Conti S**, **Rodrigues LC**, **Brown D**, **Iturriza-Gomara M**, **Gray J**, **Lopman B**. 2010. Community incidence of norovirus-associated infectious intestinal disease in England: Improved estimates using viral load for norovirus diagnosis. Am J Epidemiol **171**:1014–1022.

8. **Payne DC**, **Vinjé J**, **Szilagyi PG**, **Edwards KM**, **Staat MA**, **Weinberg GA**, **Hall CB**, **Chappell J**, **Bernstein DI**, **Curns AT**, **Wikswo M**, **Shirley SH**, **Hall AJ**, **Lopman B**, **Parashar UD**. 2013. Norovirus and Medically Attended Gastroenteritis in U.S. Children. N Engl J Med **368**:1121–1130.

9. **Belliot G**, **Lopman BA**, **Ambert-Balay K**, **Pothier P**. 2014. The burden of norovirus gastroenteritis: An important foodborne and healthcare-related infection. Clin Microbiol Infect **20**:724–730.

10. **Bartsch SM**, **Lopman BA**, **Ozawa S**, **Hall AJ**, **Lee BY**. 2016. Global economic burden of norovirus gastroenteritis. PLoS One **11**:e0151219.

11. **Ettayebi K**, **Crawford SE**, **Murakami K**, **Broughman JR**, **Karandikar U**, **Tenge VR**, **Neill FH**, **Blutt SE**, **Zeng XL**, **Qu L**, **Kou B**, **Opekun AR**, **Burrin D**, **Graham DY**, **Ramani S**, **Atmar RL**, **Estes MK**. 2016. Replication of human noroviruses in stem cell-derived human

570 enteroids. Science (80-) **353**:1387–1393.

571 12. **Jones M**, **Watanabe M**, **Zhu S**, **Graves C**, **Keyes L**, **Grau K**, **Gonzalez-Hernandez M**,
572 **Iovine N**, **Wobus C**, **Vinjé J**, **Tibbetts S**, **Wallet S**, **Karst S**. 2014. Enteric bacteria promote
573 human and mouse norovirus infection of B cells. Science (80-) **346**:755–759.

574 13. **Wobus CE**, **Karst SM**, **Thackray LB**, **Chang KO**, **Sosnovtsev S V.**, **Belliot G**, **Krug A**,
575 **Mackenzie JM**, **Green KY**, **Virgin IV HW**. 2004. Replication of Norovirus in cell culture
576 reveals a tropism for dendritic cells and macrophages. PLoS Biol **2**:e432.

577 14. **Chang K-O**, **Sosnovtsev S V.**, **Belliot G**, **King AD**, **Green KY**. 2006. Stable expression of a
578 Norwalk virus RNA replicon in a human hepatoma cell line. Virology **353**:463–473.

579 15. **Thorne LG**, **Goodfellow IG**. 2014. Norovirus gene expression and replication. J Gen Virol
580 **95**:278–291.

581 16. **Isaacs A**, **Lindenmann J**. 1988. Virus Interference: I. The Interferon. CA Cancer J Clin
582 **38**:280–290.

583 17. **Kotenko S V.**, **Gallagher G**, **Baurin V V.**, **Lewis-Antes A**, **Shen M**, **Shah NK**, **Langer JA**,
584 **Sheikh F**, **Dickensheets H**, **Donnelly RP**. 2003. IFN-λs mediate antiviral protection through a
585 distinct class II cytokine receptor complex. Nat Immunol.

586 18. **Sheppard P**, **Kindsvogel W**, **Xu W**, **Henderson K**, **Schlutsmeyer S**, **Whitmore TE**,
587 **Kuestner R**, **Garrigues U**, **Birks C**, **Roraback J**, **Ostrander C**, **Dong D**, **Shin J**, **Presnell S**,
588 **Fox B**, **Haldeman B**, **Cooper E**, **Taft D**, **Gilbert T**, **Grant FJ**, **Tackett M**, **Krivan W**,
589 **McKnight G**, **Clegg C**, **Foster D**, **Klucher KM**. 2003. IL-28, IL-29 and their class II
590 cytokine receptor IL-28R. Nat Immunol.

591 19. **De Weerd NA**, **Samarajiwa SA**, **Hertzog PJ**. 2007. Type I interferon receptors:
592 Biochemistry and biological functions. J Biol Chem.

593 20. **Sommereyns C**, **Paul S**, **Staeheli P**, **Michiels T**. 2008. IFN-lambda (IFN-λ) is expressed in a
594 tissue-dependent fashion and primarily acts on epithelial cells in vivo. PLoS Pathog **4**.

595 21. **Blazek K**, **Eames HL**, **Weiss M**, **Byrne AJ**, **Perocheau D**, **Pease JE**, **Doyle S**, **McCann F**,
596 **Williams RO**, **Udalova IA**. 2015. IFN-λ resolves inflammation via suppression of neutrophil
597 infiltration and IL-1β production. J Exp Med **212**:845–853.

598 22. **Witte K**, **Gruetz G**, **Volk HD**, **Looman AC**, **Asadullah K**, **Sterry W**, **Sabat R**, **Wolk K**.
599 2009. Despite IFN- receptor expression, blood immune cells, but not keratinocytes or
600 melanocytes, have an impaired response to type III interferons: Implications for therapeutic
601 applications of these cytokines. Genes Immun **10**:702–714.
602 23. **Dickensheets H**, **Sheikh F**, **Park O**, **Gao B**, **Donnelly RP**. 2013. Interferon-lambda (IFN-)
603 induces signal transduction and gene expression in human hepatocytes, but not in lymphocytes
604 or monocytes. J Leukoc Biol **93**:377–385.
605 24. **Ank N**, **Iversen MB**, **Bartholdy C**, **Staeheli P**, **Hartmann R**, **Jensen UB**, **Dagnaes-Hansen**
606 **F**, **Thomsen AR**, **Chen Z**, **Haugen H**, **Klucher K**, **Paludan SR**. 2008. An Important Role for
607 Type III Interferon (IFN- /IL-28) in TLR-Induced Antiviral Activity. J Immunol **180**:2474–
608 2485.
609 25. **Syedbasha M**, **Egli A**. 2017. Interferon Lambda: Modulating immunity in infectious diseases.
610 Front Immunol.
611 26. **Lee S**, **Baldridge MT**. 2017. Interferon-lambda: A potent regulator of intestinal viral
612 infections. Front Immunol.
613 27. **Hemann EA**, **Gale M**, **Savan R**. 2017. Interferon lambda genetics and biology in regulation
614 of viral control. Front Immunol **8**.
615 28. **Mordstein M**, **Neugebauer E**, **Ditt V**, **Jessen B**, **Rieger T**, **Falcone V**, **Sorgeloos F**, **Ehl S**,
616 **Mayer D**, **Kochs G**, **Schwemmle M**, **Gunther S**, **Drosten C**, **Michiels T**, **Staeheli P**. 2010.
617 Lambda Interferon Renders Epithelial Cells of the Respiratory and Gastrointestinal Tracts
618 Resistant to Viral Infections. J Virol **84**:5670–5677.
619 29. **Baldridge MT**, **Lee S**, **Brown JJ**, **McAllister N**, **Urbanek K**, **Dermody TS**, **Nice TJ**, **Virgin**
620 **HW**. 2017. Expression of *Ifnlr1* on Intestinal Epithelial Cells Is Critical to the Antiviral
621 Effects of Interferon Lambda against Norovirus and Reovirus. J Virol **91**:e02079-16.
622 30. **Nice TJ**, **Baldridge MT**, **McCune BT**, **Norman JM**, **Lazear HM**, **Artyomov M**, **Diamond**
623 **MS**, **Virgin HW**. 2015. Interferon-λ cures persistent murine norovirus infection in the absence
624 of adaptive immunity. Science (80-) **347**:269–273.
625 31. **Baldridge MT**, **Nice TJ**, **McCune BT**, **Yokoyama CC**, **Kambal A**, **Wheadon M**, **Diamond**

626 **MS**, **Ivanova Y**, **Artyomov M**, **Virgin HW**. 2014. Commensal microbes and interferon-
627 lambda determine persistence of enteric murine norovirus infection_supplemental data.
628 Science **3**:1–9.
629 32. **Rocha-Pereira J**, **Jacobs S**, **Noppen S**, **Verbeken E**, **Michiels T**, **Neyts J**. 2018. Interferon
630 lambda (IFN-λ) efficiently blocks norovirus transmission in a mouse model. Antiviral Res
631 **149**:7–15.
632 33. **Arthur SE**, **Sorgeloos F**, **Hosmillo M**, **Goodfellow I**. 2019. Epigenetic suppression of
633 interferon lambda receptor expression leads to an enhanced HuNoV replication in vitro.
634 bioRxiv 523282.
635 34. **Weber F**, **Wagner V**, **Rasmussen SB**, **Hartmann R**, **Paludan SR**. 2006. Double-Stranded
636 RNA Is Produced by Positive-Strand RNA Viruses and DNA Viruses but Not in Detectable
637 Amounts by Negative-Strand RNA Viruses. J Virol **80**:5059–5064.
638 35. **Son K-N**, **Liang Z**, **Lipton HL**. 2015. Double-Stranded RNA Is Detected by
639 Immunofluorescence Analysis in RNA and DNA Virus Infections, Including Those by
640 Negative-Stranded RNA Viruses. J Virol **89**:9383–9392.
641 36. **Andersen J**, **VanScoy S**, **Cheng TF**, **Gomez D**, **Reich NC**. 2008. IRF-3-dependent and
642 augmented target genes during viral infection. Genes Immun **9**:168–175.
643 37. **Grandvaux N**, **Servant MJ**, **tenOever B**, **Sen GC**, **Balachandran S**, **Barber GN**, **Lin R**,
644 **Hiscott J**. 2002. Transcriptional Profiling of Interferon Regulatory Factor 3 Target Genes:
645 Direct Involvement in the Regulation of Interferon-Stimulated Genes. J Virol **76**:5532–5539.
646 38. **Friedman RL**, **Manly SP**, **McMahon M**, **Kerr IM**, **Stark GR**. 1984. Transcriptional and
647 posttranscriptional regulation of interferon-induced gene expression in human cells. Cell
648 **38**:745–755.
649 39. **Reid LE**, **Brasnett AH**, **Gilbert CS**, **Porter AC**, **Gewert DR**, **Stark GR**, **Kerr IM**. 1989. A
650 single DNA response element can confer inducibility by both alpha- and gamma-interferons.
651 Proc Natl Acad Sci U S A **86**:840–4.
652 40. **Odendall C**, **Dixit E**, **Stavru F**, **Bierne H**, **Franz KM**, **Durbin AF**, **Boulant S**, **Gehrke L**,
653 **Cossart P**, **Kagan JC**. 2014. Diverse intracellular pathogens activate type III interferon

654 expression from peroxisomes. Nat Immunol **15**:717–726.

655 41. **Ding S**, **Khoury-Hanold W**, **Iwasaki A**, **Robek MD**. 2014. Epigenetic Reprogramming of the
656 Type III Interferon Response Potentiates Antiviral Activity and Suppresses Tumor Growth.
657 PLoS Biol **12**.

658 42. **Baldridge MT**, **Nice TJ**, **McCune BT**, **Yokoyama CC**, **Kambal A**, **Wheadon M**, **Diamond**
659 **MS**, **Ivanova Y**, **Artyomov M**, **Virgin HW**. 2015. Commensal microbes and interferon-λ
660 determine persistence of enteric murine norovirus infection. Science (80-) **347**:266–269.

661 43. **Rocha-Pereira J**, **Jacobs S**, **Noppen S**, **Verbeken E**, **Michiels T**, **Neyts J**. 2018. Interferon
662 lambda (IFN-λ) efficiently blocks norovirus transmission in a mouse model. Antiviral Res
663 **149**:7–15.

664 44. **Dang W**, **Xu L**, **Yin Y**, **Chen S**, **Wang W**, **Hakim MS**, **Chang KO**, **Peppelenbosch MP**,
665 **Pan Q**. 2018. IRF-1, RIG-I and MDA5 display potent antiviral activities against norovirus
666 coordinately induced by different types of interferons. Antiviral Res **155**:48–59.

667 45. **Chang K-O**. 2009. Role of Cholesterol Pathways in Norovirus Replication. J Virol **83**:8587–
668 8595.

669 46. **Naka K**, **Abe K ichi**, **Takemoto K**, **Dansako H**, **Ikeda M**, **Shimotohno K**, **Kato N**. 2006.
670 Epigenetic silencing of interferon-inducible genes is implicated in interferon resistance of
671 hepatitis C virus replicon-harboring cells. J Hepatol **44**:869–878.

672 47. **Chen Q**, **Denard B**, **Huang H**, **Ye J**. 2013. Epigenetic Silencing of Antiviral Genes Renders
673 Clones of Huh-7 Cells Permissive for Hepatitis C Virus Replication. J Virol **87**:659–665.

674 48. **Qu L**, **Murakami K**, **Broughman JR**, **Lay MK**, **Guix S**, **Tenge VR**, **Atmar RL**, **Estes MK**.
675 2016. Replication of Human Norovirus RNA in Mammalian Cells Reveals Lack of Interferon
676 Response. J Virol **90**:8906–8923.

677 49. **Schmittgen TD**, **Livak KJ**. 2008. Analyzing real-time PCR data by the comparative CT
678 method. Nat Protoc **3**:1101–1108.

679 50. **Fernandez-vega V**, **Sosnovtsev S V**, **King AD**, **Mitra T**, **Gorbalenya A**, **Green KY**. 2004.
680 Norwalk Virus N-Terminal Nonstructural Protein Is Associated with Disassembly of the Golgi
681 Complex in Transfected Cells. J Virol **78**:4827–4837.

682 51. **Pervolaraki K**, **Stanifer ML**, **Münchau S**, **Renn LA**, **Albrecht D**, **Kurzhals S**, **Senís E**,
683 **Grimm D**, **Schröder-Braunstein J**, **Rabin RL**, **Boulant S**. 2017. Type I and type III
684 interferons display different dependency on mitogen-activated protein kinases to mount an
685 antiviral state in the human gut. Front Immunol **8**.
686
687

Fig. 1

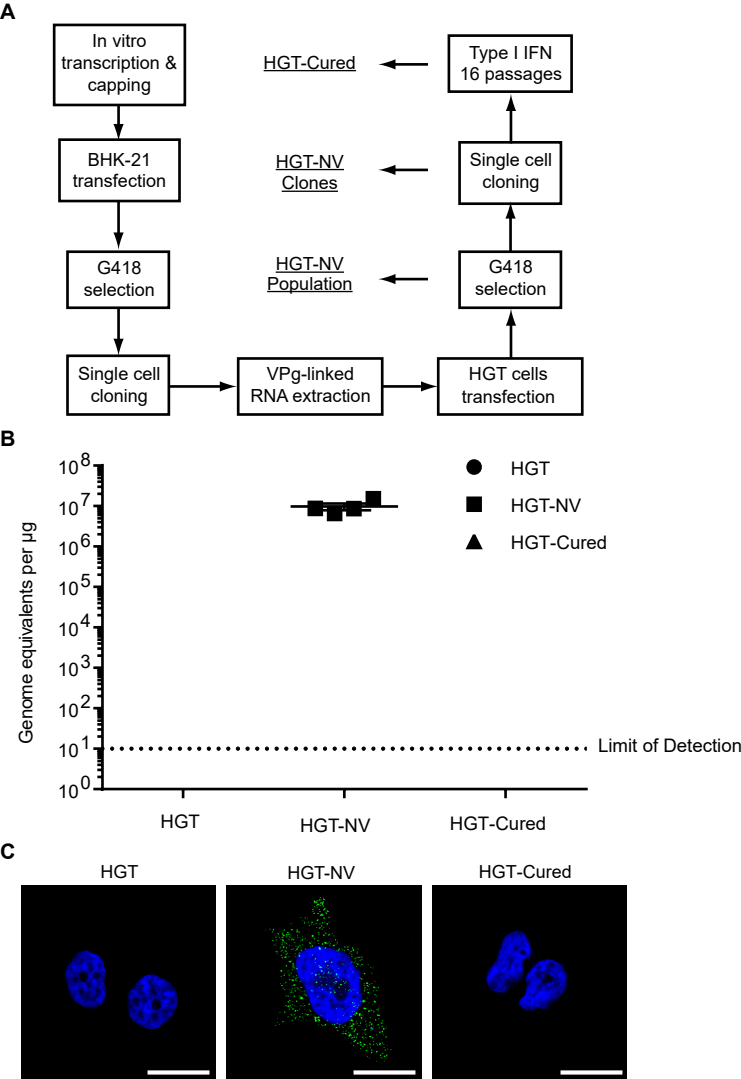
A
In vitro transcription & capping
BHK-21 transfection
G418 selection
Single cell cloning
VPg-linked RNA extraction
HGT cells transfection
G418 selection
Single cell cloning
HGT-NV Population
HGT-NV Clones
HGT-Cured
Type I IFN 16 passages
B
Genome equivalents per µg
HGT
HGT-NV
HGT-Cured
Limit of Detection
C
HGT
HGT-NV
HGT-Cured

Fig. 2

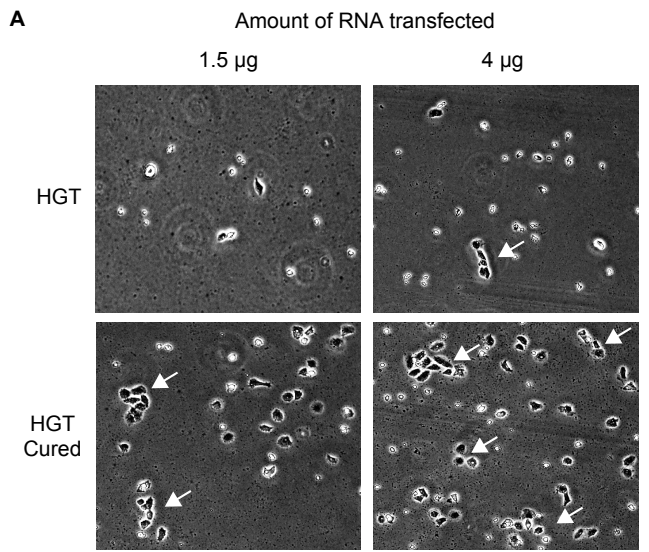
A
Amount of RNA transfected
1.5 µg
4 µg
HGT
HGT Cured
B
HGT
HGT-Cured
****
****
Fold change in viral RNA genome equivalents relative to day 0
25
20
15
10
5
0
1
2
3
5
6
Days post selection in G418

Fig. 3

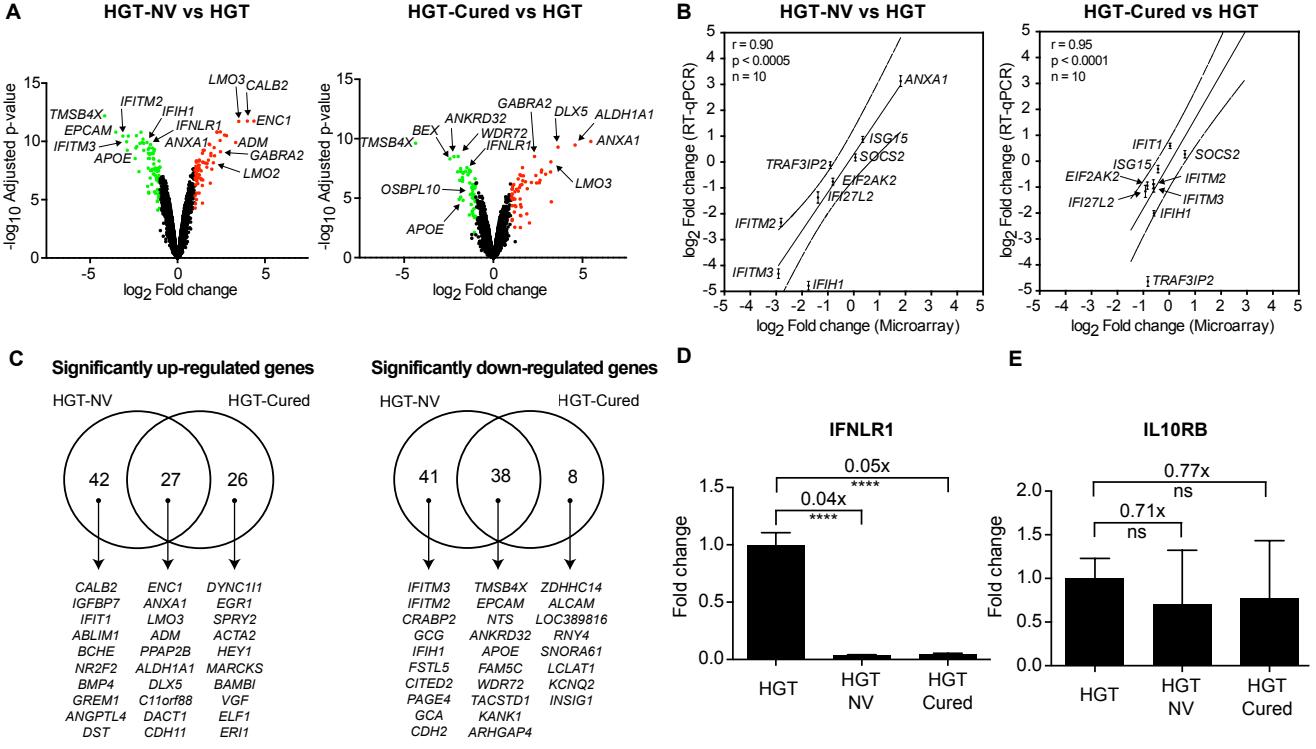
A
HGT-NV vs HGT
HGT-Cured vs HGT
-log10 Adjusted p-value
log2 Fold change
TMSB4X
EPCAM
IFITM3
APOE
IFITM2
IFIH1
IFNLR1
ANXA1
LMO3
CALB2
ENC1
ADM
GABRA2
LMO2
BEX
ANKRD32
WDR72
GABRA2
DLX5
ALDH1A1
OSBPL10
B
HGT-NV vs HGT
HGT-Cured vs HGT
r = 0.90
p < 0.0005
n = 10
r = 0.95
p < 0.0001
n = 10
log2 Fold change (RT-qPCR)
log2 Fold change (Microarray)
ANXA1
ISG15
SOCS2
TRAF3IP2
EIF2AK2
IFI27L2
IFITM2
IFITM3
IFIH1
IFIT1
ISG15
EIF2AK2
IFITM2
IFITM3
IFIH1
IFI27L2
TRAF3IP2
C
Significantly up-regulated genes
HGT-NV
HGT-Cured
42
27
26
CALB2
IGFBP7
IFIT1
ABLIM1
BCHE
NR2F2
BMP4
GREM1
ANGPTL4
DST
ENC1
ANXA1
LMO3
ADM
PPAP2B
ALDH1A1
DLX5
C11orf88
DACT1
CDH11
DYNC1I1
EGR1
SPRY2
ACTA2
HEY1
MARCKS
BAMBI
VGF
ELF1
ERI1
Significantly down-regulated genes
HGT-NV
HGT-Cured
41
38
8
IFITM3
IFITM2
CRABP2
GCG
IFIH1
FSTL5
CITED2
PAGE4
GCA
CDH2
TMSB4X
EPCAM
NTS
ANKRD32
APOE
FAM5C
WDR72
TACSTD1
KANK1
ARHGAP4
ZDHHC14
ALCAM
LOC389816
RNY4
SNORA61
LCLAT1
KCNQ2
INSIG1
D
IFNLR1
0.05x
****
0.04x
****
Fold change
HGT
HGT NV
HGT Cured
E
IL10RB
0.77x
ns
0.71x
ns
Fold change
HGT
HGT NV
HGT Cured

Fig. 4

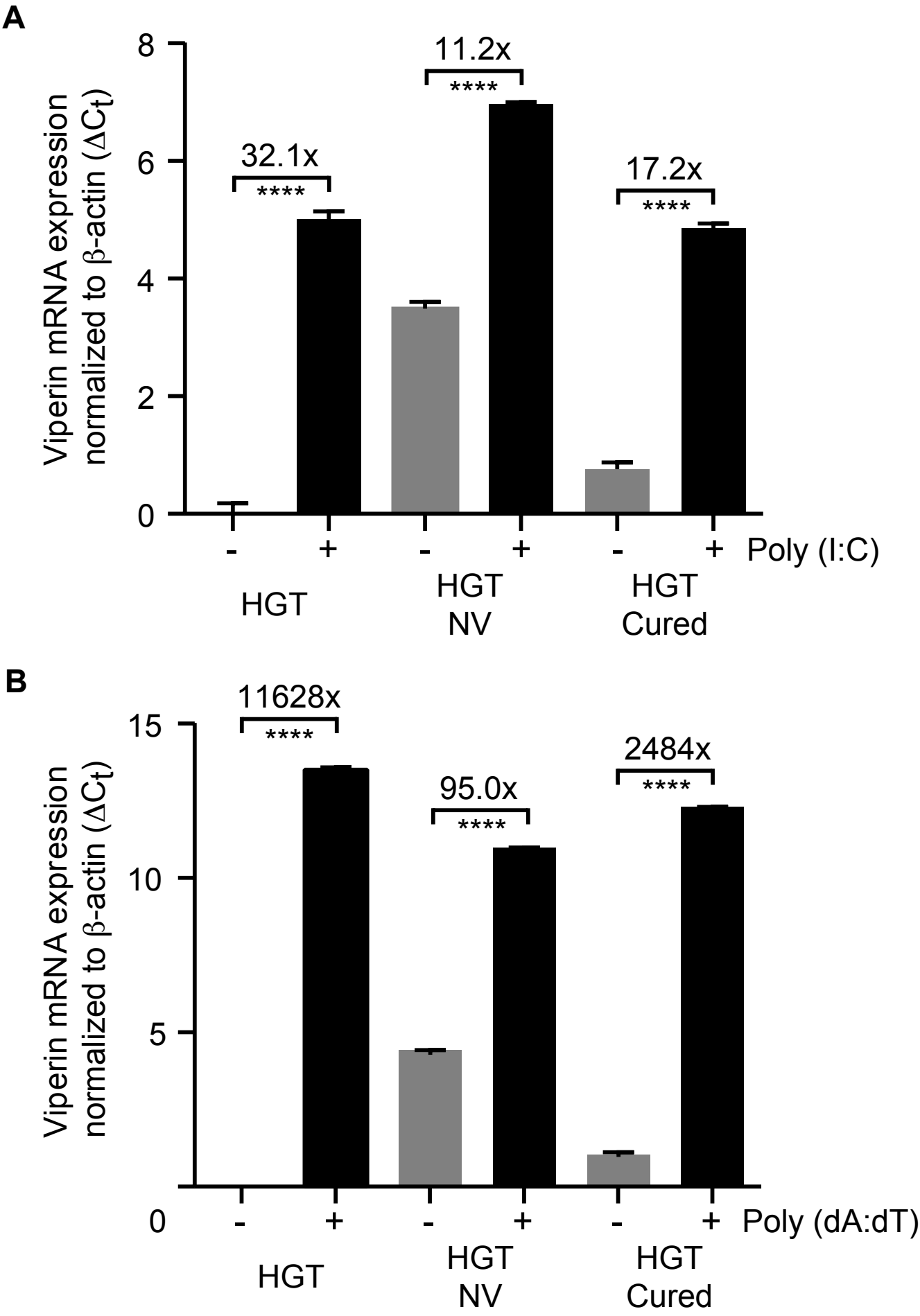
A
Viperin mRNA expression normalized to β-actin (ΔCt)
8
6
4
2
0
32.1x
****
11.2x
****
17.2x
****
- + - + - +
Poly (I:C)
HGT
HGT NV
HGT Cured
B
Viperin mRNA expression normalized to β-actin (ΔCt)
15
10
5
0
11628x
****
95.0x
****
2484x
****
- + - + - +
Poly (dA:dT)
HGT
HGT NV
HGT Cured

Fig. 5

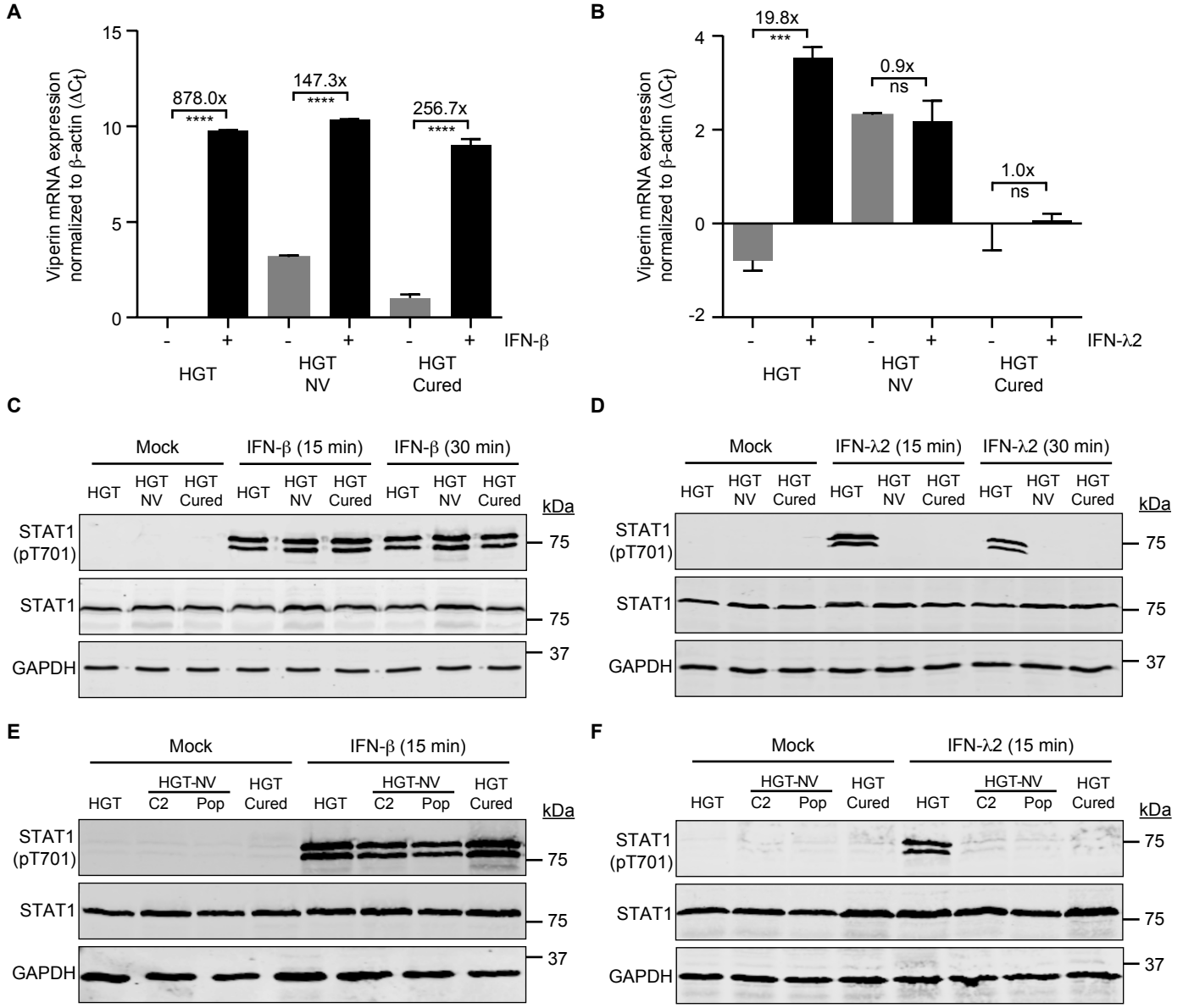
A
Viperin mRNA expression normalized to β-actin (ΔCt)
878.0x
****
147.3x
****
256.7x
****
IFN-β
HGT
HGT NV
HGT Cured
B
Viperin mRNA expression normalized to β-actin (ΔCt)
19.8x
***
0.9x
ns
1.0x
ns
IFN-λ2
HGT
HGT NV
HGT Cured
C
Mock
IFN-β (15 min)
IFN-β (30 min)
HGT
HGT NV
HGT Cured
kDa
STAT1 (pT701)
STAT1
GAPDH
75
75
37
D
Mock
IFN-λ2 (15 min)
IFN-λ2 (30 min)
HGT
HGT NV
HGT Cured
kDa
STAT1 (pT701)
STAT1
GAPDH
75
75
37
E
Mock
IFN-β (15 min)
HGT
HGT-NV
C2
Pop
HGT Cured
kDa
STAT1 (pT701)
STAT1
GAPDH
75
75
37
F
Mock
IFN-λ2 (15 min)
HGT
HGT-NV
C2
Pop
HGT Cured
kDa
STAT1 (pT701)
STAT1
GAPDH
75
75
37

Fig. 6

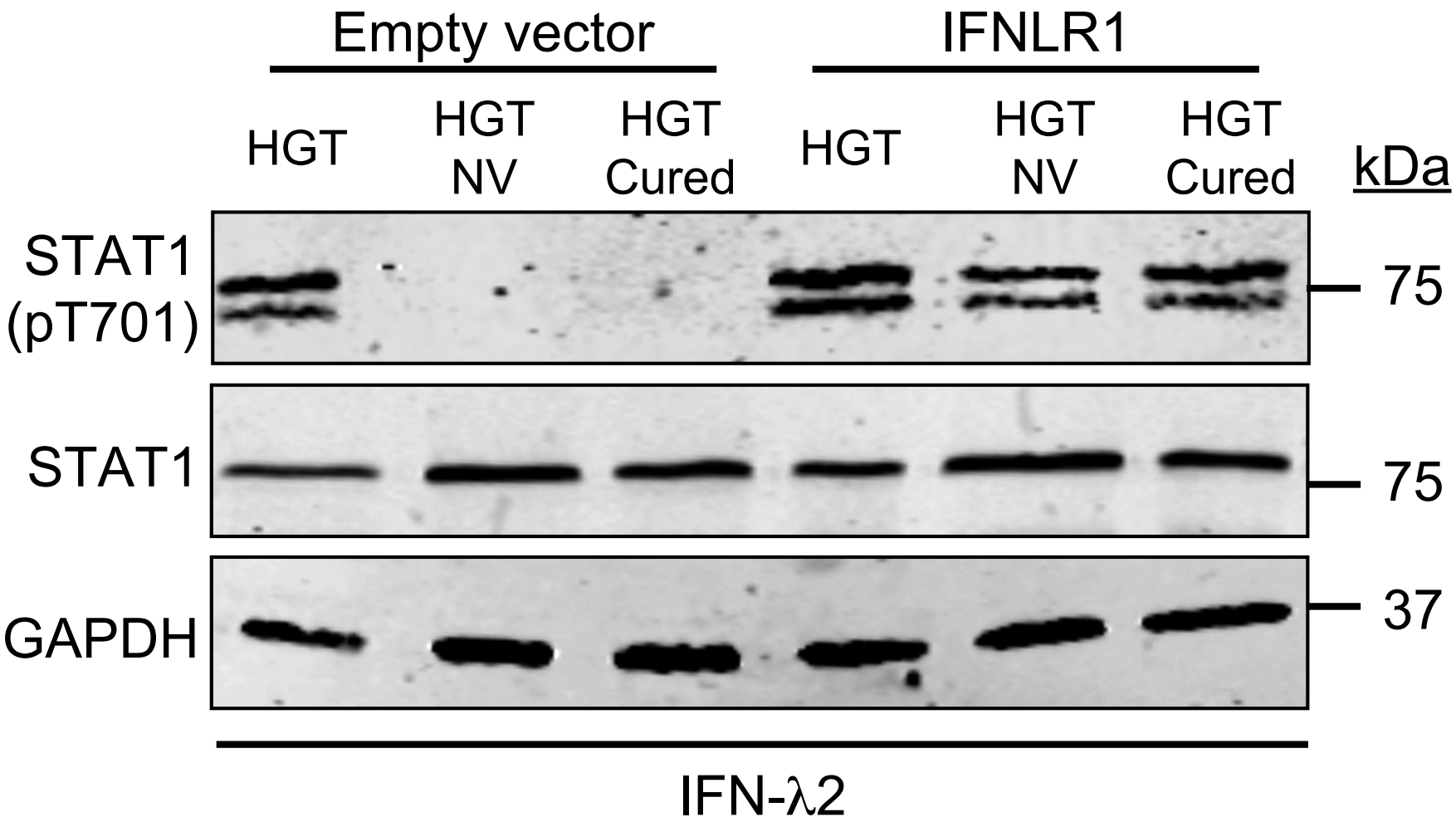
Empty vector
IFNLR1
HGT
HGT NV
HGT Cured
HGT
HGT NV
HGT Cured
kDa
STAT1 (pT701)
75
STAT1
75
GAPDH
37
IFN-λ2

Fig. 7

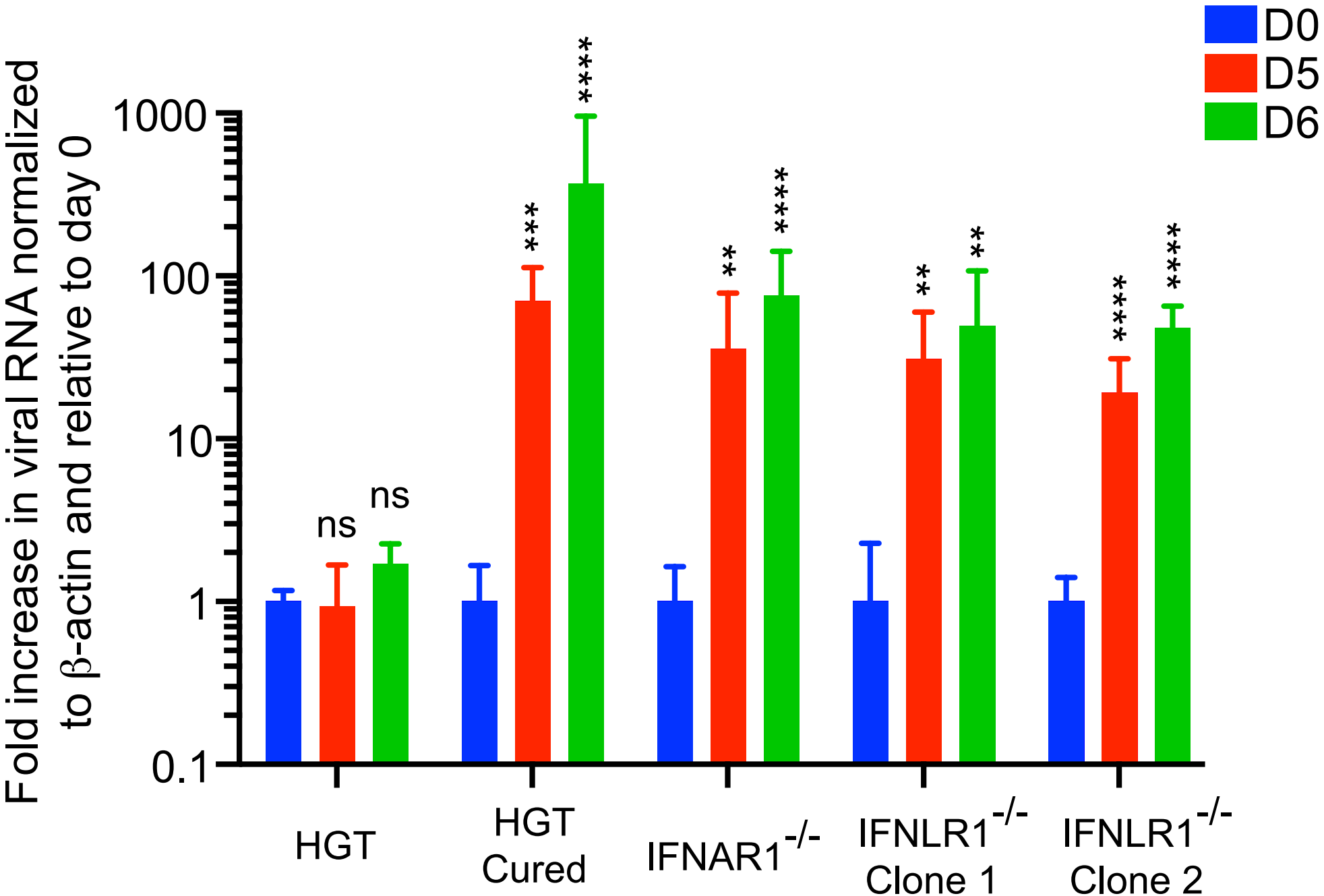
D0
D5
D6
Fold increase in viral RNA normalized to β-actin and relative to day 0
1000
100
10
1
0.1
ns
ns
***
*****
**
*****
**
**
*****
*****
HGT
HGT Cured
IFNAR1-/-
IFNLR1-/- Clone 1
IFNLR1-/- Clone 2

Fig. 8

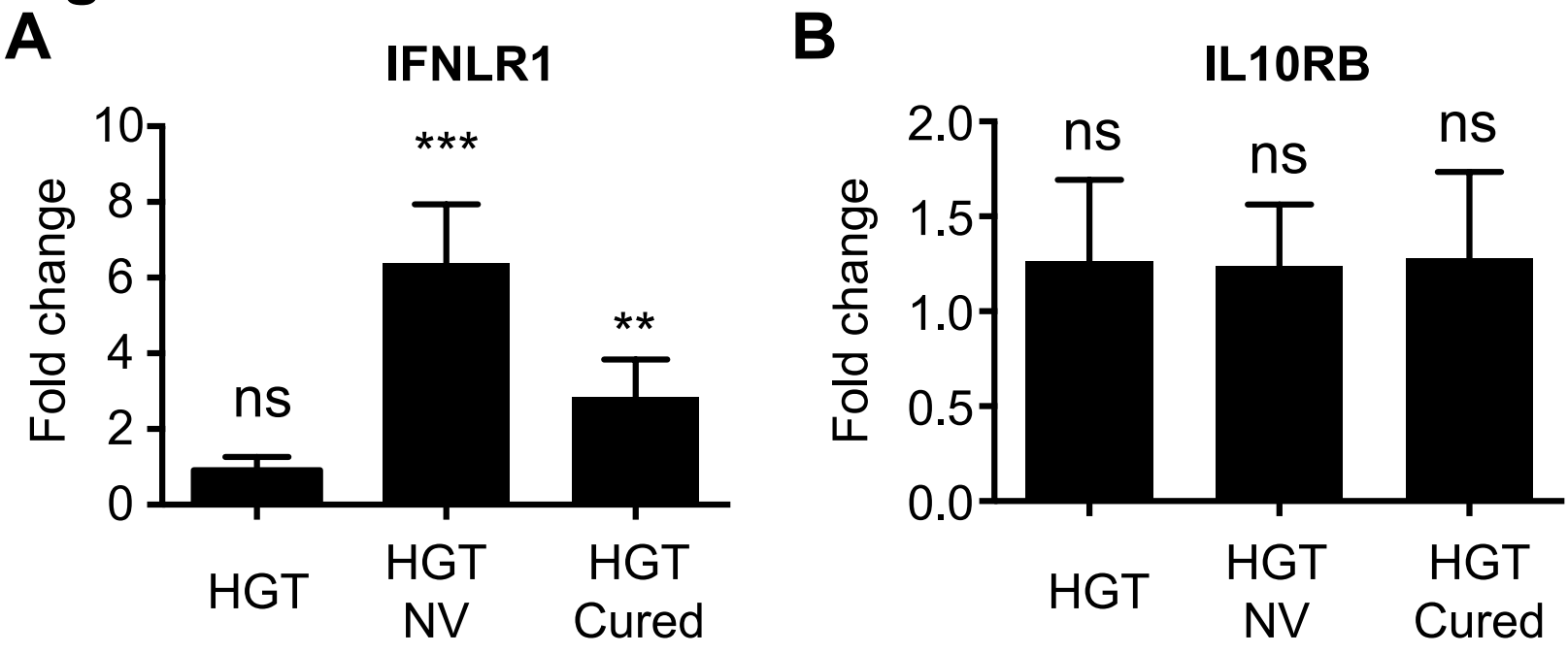
A
IFNLR1
Fold change
10
8
6
4
2
0
***
**
ns
HGT
HGT NV
HGT Cured
B
IL10RB
Fold change
2.0
1.5
1.0
0.5
0.0
ns
ns
ns
HGT
HGT NV
HGT Cured